Nanoscale Advances

ROYAL SOCIETY OF CHEMISTRY

PAPER

View Article Online
View Journal | View Issue

Cite this: *Nanoscale Adv.*, 2022, **4**, 4617

Highly biocompatible chlorin e6-poly(dopamine) core–shell nanoparticles for enhanced cancer phototherapy†

Shilin Chen,[a] Yihang Jiang,[a] Miaozhaung Fan,[a] Xinmeng Zhang,[a] Ying Zhang,[a] Ting Chen,[b] Chengbin Yang,[a] Wing-Cheung Law,*[b] Zhourui Xu*[a] and Gaixia Xu*[a]

Received 31st July 2022
Accepted 14th September 2022

DOI: 10.1039/d2na00504b

rsc.li/nanoscale-advances

Cancer is a life-threatening disease worldwide. Although several approaches, such as surgery, chemotherapy, and radiotherapy, have been proven effective for many patients in clinics, they usually suffer from drug resistance, severe toxic-side effects, patient discomfort, and sometimes, unsatisfactory efficacies. In recent years, phototherapy, as a less invasive but effective therapeutic method, has brought hope for cancer treatment. However, most reported photo-therapeutic agents are constructed using complex components with non-negligible toxicity risk, thus retarding the start of their clinical trials. To address this issue, herein, biocompatible photothermal/photodynamic dual-mode therapeutic nanoparticles (CBP NPs) were successfully designed and constructed based on the Food and Drug Administration (FDA)-approved ingredients, chlorin e6 (Ce6) and poly(dopamine) (PDA). Upon light irradiation, hyperthermia was induced and reactive oxygen species (ROS) were generated simultaneously by CBP NPs, contributing to synergistic phototherapy toward cancer. The *in vitro* and *in vivo* experiments have demonstrated well the antitumor effect of CBP NPs. More importantly, CBP NPs are completely harmless and degradable *in vivo*. Together, the CBP NPs developed by us are an ideal candidate for the enhanced phototherapy of tumors, which holds great potential for future clinical translation.

1 Introduction

Cancer is one of the major diseases that seriously threaten human health in the world.[1–3] Its notorious features, including rapid deterioration and high mortality, have brought severe economic burden and social pressure to patients and society.[4] According to the World Health Organization, the number of cancer deaths worldwide is expected to exceed 10 million in 2022.[5] Although the current standard of care, including surgery, chemotherapy, and radiotherapy, has been proved to be effective in clinics, their intrinsic limitations,[6–8] such as invasive therapy, drug resistance, severe toxic-side effects, and patient discomfort, remain great challenges and hugely affect the therapeutic outcomes.[9,10] Thus, it is of great significance to develop novel treatment alternatives which could address the current concerns.

Phototherapy has received extensive attention in the biomedical field owing to its unique advantages, including negligible toxicity, superior spatial and temporal control, repeatable treatment, wide anti-tumor spectrum, and easy operation.[11] Briefly, phototherapies that involve the administration of exogenous therapeutic agents under light radiation can be categorized as photodynamic therapy (PDT) and photothermal therapy (PTT), among which PDT relies on the localized chemical damage in the target lesions while PTT exerts a therapeutic effect *via* localized thermal damage.[12–16] However, as a single-mode treatment method, PDT or PTT alone often suffers from low therapeutic efficacy, due to insufficient ROS production and low heat conversion efficiency (HCE). Although the therapeutic effect can be enhanced by increasing the concentration of photo-therapeutic agents or laser power, the safety risk may increase drastically owing to dosage-dependent toxicity and collateral damage.[17,18] Fortunately, it has been reported that dual-mode phototherapy combining PDT and PTT can significantly improve the therapeutic effect *via* a synergistic effect. On one hand, ROS can denature heat shock proteins and undermine cellular thermal resistance;[19] on the other hand, localized heat can increase the cellular uptake of NPs and oxygen supply, thereby strengthening the therapeutic effect of PDT.[20,21] Hence, developing phototherapy combining PDT and PTT is a promising and feasible treatment strategy.

[a]*Guangdong Key Laboratory for Biomedical Measurements and Ultrasound Imaging, School of Biomedical Engineering, Health Science Center, Shenzhen University, Shenzhen 518060, China. E-mail: xuzhouray@szu.edu.cn; xugaixia@szu.edu.cn*

[b]*Department of Industrial and Systems Engineering, The Hong Kong Polytechnic University, Hong Kong. E-mail: roy.law@polyu.edu.hk*

† Electronic supplementary information (ESI) available. See https://doi.org/10.1039/d2na00504b

Over the past decade, great strides have been made in the exploitation of new photo-therapeutic agents for cancer treatments. These materials are generally fabricated based on nanocarbons, plasmonic nanostructures, two-dimensional nanoplates, and long-conjugation organic probes, which have been proven effective in tumor ablation.[22–27] However, several challenges have restricted their entrance into the clinical stage. First and foremost, most dual-mode photo-therapeutic agents are prepared using inorganic nanomaterials, which are not easily metabolized from the body, resulting in accumulation of toxicity. Such toxicity risk could be more severe when heavy metal ions were included.[28] Quite a few researchers have questioned the safety concerns of photo-therapeutic agents, such as gold NPs, nanocarbons, and black phosphorus, which cause a non-negligible risk in the pro-inflammatory response of macrophages, reduced cell activity, and even genotoxicity.[29–32] In addition, complex methods with multiple steps and time-consuming processes are always required, leading to large batch-to-batch differences and unreliable properties. Therefore, to thrust phototherapy into a more practical stage and make contributions to society, it is of great necessity and significance to develop safe and reliable therapeutic agents with carefully selected ingredients.

In this work, CBP NPs, a dual-mode core–shell photo-therapeutic agent, were successfully designed and fabricated, based on the FDA-approved ingredients, Ce6 and PDA. Ce6 is a highly effective photosensitizer, which is almost harmless to the human body.[33] Dopamine is a neurotransmitter in the human body, which has good biocompatibility and promising HCE.[34] By integrating Ce6 and PDA into NPs with a modified precipitation method, we obtained CBP NPs as a novel pho-therapeutic agent, which exhibited narrow size distribution, good stability, and synergistic phototherapy. The *in vitro* and *in vivo* experiments revealed the highly efficient anti-tumor effect of CBP NPs even under low material concentration (20 μM) and low power densities of lasers (1 W cm^{-2} for 808 nm and 50 mW cm^{-2} for 660 nm). The biocompatibility of the material was verified systematically by blood routine tests, blood biochemistry tests, and histological examination. Therefore, the nanomaterial proposed in this work with high biocompatibility and strong phototherapeutic effect possesses great potential in future clinical translation.

2 Materials and methods

2.1 Chemicals and materials

Bovine Serum Albumin (BSA) and 9,10-anthracenediyl-bis(-methylene)dimalonic acid (ABDA) were purchased from Sigma Aldrich Co., Ltd. Ce6, dopamine hydrochloride, tetrahydrofuran (THF), and dimethyl sulfoxide (DMSO) were supplied by Shanghai Maclin Biochemical Technology Co., Ltd. Tris-buffer was purchased from Shanghai Sangon Biotech Co., Ltd. All chemicals were used without further purification.

2.2 Preparation of chlorin e6-poly(dopamine) core–shell NPs

First, the nanoprecipitation method was used to synthesize Ce6-BSA NPs. Then, dopamine was polymerized on the surface of Ce6-BSA NPs under alkaline conditions. Finally, we obtained the CBP NPs. The specific experimental processes are as follows:

(1) BSA (5 mg) was dissolved in deionized water (5 mL) and Ce6 (0.25 mg) was dissolved in tetrahydrofuran (0.5 mL); (2) the THF solution of Ce6 was slowly added to BSA solution continuously under sonication at room temperature for 5 min; (3) the Ce6-BSA NPs were obtained by ultrafiltration at 4400 rpm for 20 min; (4) the obtained NPs were dispersed in tris-buffer (10 μM, pH = 8.0), then dopamine hydrochloride was added into the mixture (4 mg mL^{-1}), and kept stirring for 24 h at room temperature and under dark conditions. (5) Finally, the CBP NPs were obtained by ultrafiltration at 4400 rpm for 20 min. After purification, the obtained CBP NPs were redispersed in deionized water or PBS solution for further use.

2.3 Characterization of CBP NPs

The transmission electron microscopy images of CBP NPs were captured using a HT7700 transmission electron microscope (Hitachi, Ltd.). The UV-vis-NIR absorption spectrum was measured on a TP-720 spectrometer (Tianjin Tuopu Instrument Co., Ltd.). The *in vivo* and *in vitro* photothermal performances of samples were evaluated using an NIR Laser (Changchun Leishi Photo-Electric Technology Co., Ltd.) and FLIR A300 Infrared Thermal Imaging camera (FLIR Systems Co., Ltd.). The hydrodynamic size and stability of the samples were measured using the Zetasizer-Nano-ZS-90 dynamic light scattering equipment (Malvern Panalytical, Ltd.).

2.4 Measurement of photodynamic effects

To evaluate the photodynamic performance, we measured the ROS generation of CBP NPs using ABDA as an indicator. The CBP NP (20 μM) dispersion in PBS containing 50 μM ABDA was irradiated using a 660 nm laser with a power density of 50 mW cm^{-2}, an 808 nm laser with a power density of 1 W cm^{-2}, or a combined laser of 660 nm (50 mW cm^{-2}) and 808 nm (1 W cm^{-2}) simultaneously, respectively. The degradation of ABDA was measured at different time points (0–10 min).

2.5 Measurement of photothermal effects

To measure the photothermal effects, a series of CBP NP dispersions with different concentrations were added into plastic centrifugal tubes. The tubes were exposed to 808 nm laser irradiation with the same power density (1 W cm^{-2}). An infrared thermal imaging camera was used to record the temperature variation.

2.6 *In vitro* Ce6 release behavior of CBP NPs

The Ce6 release from CBP NPs was investigated using the dynamic dialysis method. In brief, CBP NPs were loaded into a dialysis bag, immersed in 20 mL of PBS (pH of 7.4 and 5.0), and stirred at 37 °C. Photothermal treatment was applied to the sample at predetermined time points. At different time points, an aliquot of buffer was withdrawn to determine the Ce6 concentration using a UV-vis spectrophotometer followed by

replenishment with a fresh medium. The cumulative Ce6 release was then calculated and drawn.

2.7 Cell culture

The murine breast cancer cell line (4T1), human breast cancer cell line (MCF-7), human cervical cancer cell line (HeLa), and human breast health cell line (MCF-10A) were cultured in DMEM medium containing 10% fetal bovine serum (FBS) and 1% penicillin–streptomycin solution (PS) in a cell incubator (37 °C, 5% CO_2).

2.8 Cytotoxicity of CBP NPs

In vitro cytotoxicity of CBP NPs was evaluated by using HeLa cells, MCF-7 cells, MCF-10A cells, and 4T1 cells. These four kinds of cells were seeded in 96-well plates at a density of 5000 cells per well and grown in a cell incubator (37 °C and 5% CO_2) for 24 h. Then the original medium was replaced by the medium containing different concentrations of CBP NPs (1–200 μM). After incubation for 24 h, the medium with CBP NPs was removed and 90 μL of fresh culture medium and 10 μL of Cell Counting Kit-8 (CCK-8) solution were added to each well and incubated for another 20–60 min. At the end of incubation, the absorbance of the solution in each well was measured using a microplate reader (Bio-tek, Epoch-2) at a wavelength of 450 nm. The cell viability rate can be calculated using eqn (1)

$$\text{Cell viability } (\%) = \frac{\text{OD}_{\text{sample}} - \text{OD}_{\text{blank}}}{\text{OD}_{\text{control}} - \text{OD}_{\text{blank}}} \times 100 \quad (1)$$

where $\text{OD}_{\text{sample}}$ and $\text{OD}_{\text{control}}$ are the absorbance of experimental cells (with CBP NPs added) and control cells (without CBP NPs), respectively. OD_{blank} is the absorbance of the CCK-8 solution itself at 450 nm. All experiments were conducted in parallel three times and the mean value ± standard deviation (SD) was presented as calculated.

2.9 *In vitro* cellular uptake evaluation

To evaluate the uptake of CBP NPs by 4T1 cells, confocal microscopy was used to observe the fluorescence, and flow cytometry was used to quantitatively analyze the uptake rate. 4T1 cells were seeded in confocal dishes at a density of 1×10^5 cells and grown in a cell incubator (37 °C and 5% CO_2) for 24 h. Then the original medium was replaced by the medium containing CBP NPs (20 μM of Ce6 and 50 ppm of PDA). After incubation for different times (0–24 h), the paraformaldehyde solution was added to the confocal dishes, and the cells were fixed under darkness for 10–15 min, and then 2–3 drops of 4,6-diamino-2-phenyl indole (DAPI) solution were added to stain the nuclei. After washing with PBS three times, 1 mL of PBS was added to each confocal dish and the cell samples were imaged using a confocal fluorescence microscope. Meanwhile, fluorescence in the cell samples after incubation with CBP NPs for 4 h (without cell fixation) was detected by flow cytometry for quantitative analysis of cellular uptake.

2.10 *In vitro* phototherapy and live/dead double staining

To evaluate the photo-therapeutic effect on treated cell samples. CCK-8 was applied to different groups of cell samples. Five experimental groups and one control group were set up. Cell samples were co-incubated with CBP NPs (20 μM of Ce6 and 50 ppm of PDA) for 4 h and then irradiated with an 808 nm laser, a 660 nm laser, or the combination of the two lasers (double laser irradiation), respectively. The power densities of the 808 nm and 660 nm lasers used in this experiment were 1 W cm^{-2} and 50 mW cm^{-2}, respectively, and the time of laser irradiation was 5 min. After treatment, the original medium was replaced by the fresh medium containing 10% FBS and 1% PS and the cell samples were cultured in an incubator for 4 h. The cell viability then was determined by CCK-8, according to the above-mentioned procedure.

To visualize the photo-therapeutic effect on treated cell samples. Calcein-AM and PI were applied to different groups of cell samples. After treatment for 4 h, 2 μL working solutions of calcein-AM and PI were added to each cell culture dish. After incubation for 20 min and replacement of the medium with a fresh culture medium, the cell samples were imaged using a fluorescent microscope. Calcein-AM is a cell-permeable and non-fluorescent compound that can emit green fluorescence when it enters metabolically active cells. PI is a fluorescent nucleic acid stain that can only permeate damaged cell membranes and emit red fluorescence.

2.11 Calculation of the combined index

To judge the synergy between PDT and PTT based on CBP NPs under double laser irradiation, the combined index (CI) value was calculated based on the IC50 value of PDT, PTT, and PDT&PTT by using eqn (2):

$$\frac{a}{A} + \frac{b}{B} = \text{CI} \quad (2)$$

where a is the dose of CBP NPs for PTT in the combined phototherapy to achieve IC50, b is the dose of CBP NPs for PDT in the combined phototherapy to achieve IC50; A is the dose of CBP NPs for PTT alone to achieve IC50; B is the dose of CBP NPs for PDT alone to achieve IC50.

2.12 Hemolysis test

The impact of CBP NPs on red blood cells (RBCs) of mice was evaluated by the standard hemolysis test. A volume of 500 μL of fresh blood was taken from mice and mixed with 5 mL of PBS solution. The blood was mixed gently and centrifuged at 3000 rpm for 20 min. After discarding the supernatant, the RBCs were re-suspended in PBS solution and purified several times. The final working suspension containing 5% (v/v) RBCs in a PBS solution was used for the hemolysis test. To evaluate the hemolysis effect, CBP NPs with different concentrations (0, 1, 10, 20, 50, 100, 200 μM) were co-incubated with RBC suspension for 4 h at room temperature (total volume was 1 mL). After incubation, the samples were centrifuged again and 100 μL of supernatants were extracted. The absorbance was measured at the wavelength of 540 nm for the quantitative determination of

hemoglobin content in supernatants. Meanwhile, we mixed deionized water and PBS solution with the RBC suspension as the positive control and negative control, respectively. Finally, the percentage of hemolysis was calculated according to eqn (3):

$$\text{Hemolysis rate } (\%) = \frac{\text{ABS}_{\text{sample}} - \text{ABS}_{\text{control-neg}}}{\text{ABS}_{\text{control-pos}} - \text{ABS}_{\text{control-neg}}} \times 100 \quad (3)$$

where $\text{ABS}_{\text{sample}}$, $\text{ABS}_{\text{control-neg}}$, and $\text{ABS}_{\text{control-pos}}$ are the optical density of tested samples, negative control, and positive control, respectively.

2.13 *In vivo* cancer phototherapy

In order to evaluate the photo-therapeutic effect of CBP NPs on tumors *in vivo*, we conducted experiments with Balb/C mice. All the mice were purchased from Guangdong Medical Laboratory Animal Center (No. 44007200082293) and all the animal experiments conform to the guidelines of the University Animal Care and Use Committee. The tumor-bearing mice were established by subcutaneous injection of 4T1 cells (murine breast cancer cell line, 1×10^6 cells) onto the right leg, where the tumors grew for about 10 days and reached a size of about 100 mm^3. Then, the 4T1 tumor-bearing Balb/C mice were randomly divided into 6 groups. The treatments are as follows: (1) injection of PBS without irradiation; (2) injection of PBS with a combination of 660 nm and 808 nm irradiation; (3) injection of CBP NPs without irradiation; (4) injection of CBP NPs with 660 nm irradiation alone; (5) injection of CBP NPs with 808 nm irradiation alone; (6) injection of CBP NPs with a combination of 660 nm and 808 nm irradiation. The intra-tumoral injection dose of CBP NPs was 10 mg kg^{-1}. The irradiation power of 660 nm and 808 nm laser was 50 mW cm^{-2} and 1 W cm^{-2} respectively. The irradiation time of each group was 5 min, and one injection and phototherapy were only performed on day 0. The body weight and tumor volumes were recorded every two days. Tumor volume was calculated according to eqn (4):

$$v = \frac{A \times B^2}{2} \quad (4)$$

where v is the volume of the tumor, and A and B are the long and short axis of the tumor, respectively. Moreover, the tumor tissues in each group were harvested from mice 24 h after the first treatment and were also dissected and fixed with paraformaldehyde used for hematoxylin and eosin (H&E) and terminal deoxynucleotidyl transferase-mediated dUTP-biotin nick end labeling (TUNEL) staining assay. The cell morphology was observed under a microscope.

2.14 *In vivo* biosafety test

To further evaluate the biosafety of CBP NPs *in vivo*, we conducted experiments with Balb/C mice. The mice were randomly divided into four groups and were injected with PBS and CBP NP suspensions at a concentration of 1 mg kg^{-1}, 10 mg kg^{-1}, and 30 mg kg^{-1} *via* the tail vein, respectively. Then the body weights of the mice were recorded every two days. The blood of the mice in each group was collected for blood routine and biochemical analysis after 14 days. The heart, liver, spleen, lungs, and kidneys of mice in each group were collected and each organ was weighed. The organ coefficient was calculated according to eqn (5):

$$\text{Organ coefficient} = \frac{W_{\text{organ}}}{W_{\text{body}}} \quad (5)$$

where W_{organ} and W_{body} are the weight of the organ and the body of mice, respectively. The organs in each group were dissected and fixed with paraformaldehyde for H&E staining essay. The cell morphology was observed under a microscope.

2.15 Statistical analysis

Statistical results of all data are presented as mean value ±SD. The *T*-test was used to compare the results between two groups. No statistical difference is represented by ns.

3 Results and discussion

3.1 Synthesis and characterization of CBP NPs

The preparation procedure of CBP NPs and the photo-therapeutic strategy are demonstrated in Scheme 1. Ce6-BSA NPs were first synthesized by nanoprecipitation, and then dopamine was polymerized on the surface of NPs under alkaline conditions. After that, CBP NPs were obtained.

The morphology, size distribution, and stability of CBP NPs were characterized by TEM and DLS. The TEM image showed approximately spherical CBP NPs with average diameters of about 60 nm (Fig. 1a) with nearly uniform size. The average hydrodynamic diameter of CBP NPs was 80.7 ± 6.6 nm with a polydispersity index (PDI) of 0.148 (Fig. 1b). Such a size difference can be explained by the dehydrated and hydrated state of NPs. In order to evaluate the stability of CBP NPs, the hydrodynamic diameter was measured for 14 continuous days in PBS. As shown in Fig. 1c, there was no significant change in particle size within 14 days and there was only a slight increase in PDI that remained below 0.3. The colloidal stability was further confirmed by measuring the hydrodynamic size and zeta potential of CBP NPs in different biological fluids within a continuous period (Fig. S1†).

To verify the synthesis of Ce6-BSA NPs and the polymerization of PDA, the UV-vis-NIR absorption spectra of Ce6-BSA, PDA, and CBP NPs were recorded. As illustrated in Fig. 1d, absorption peaks of Ce6-BSA NPs appeared at the wavelengths of 405 nm and 675 nm, corresponding to the characteristic absorption peaks of Ce6, which indicated that Ce6-BSA NPs were synthesized successfully. Compared with Ce6-BSA, the absorption spectrum of CBP NPs between 200–1000 nm was elevated, following the trend of the absorption spectrum of PDA, which indicated that PDA was polymerized successfully. The above results confirmed that the synthesis of CBP NPs was successful.

3.2 Photodynamic and photothermal effect of CBP NPs

The production of ROS is the key parameter of PDT. Ce6 can efficiently produce ROS under the irradiation of a 660 nm laser for PDT. It has been reported that the photothermal effect can be used to enhance ROS production. Hence, we have measured

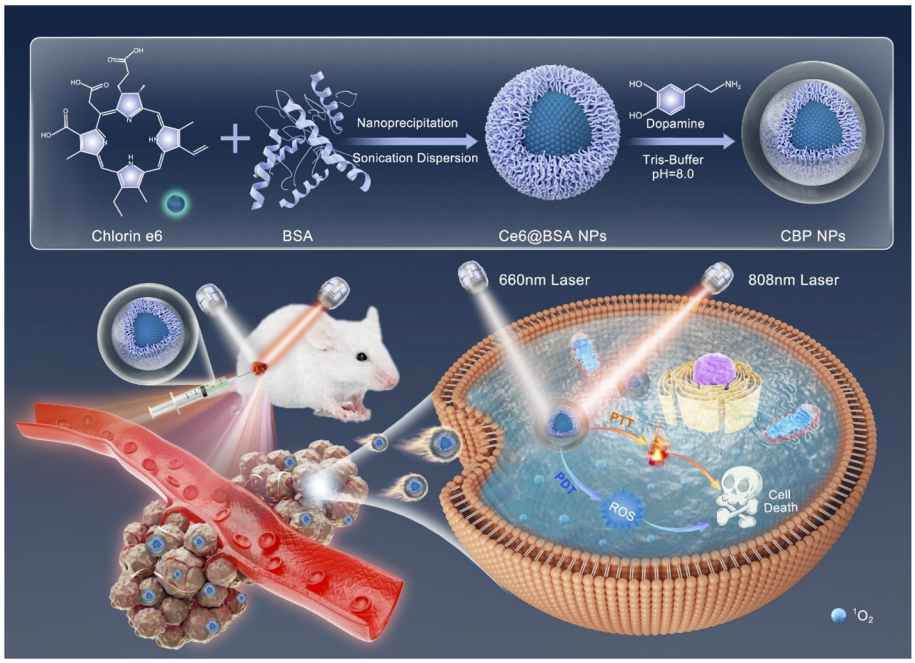

Scheme 1 Schematic illustration of the design and preparation of CBP NPs for synergistic PTT/PDT.

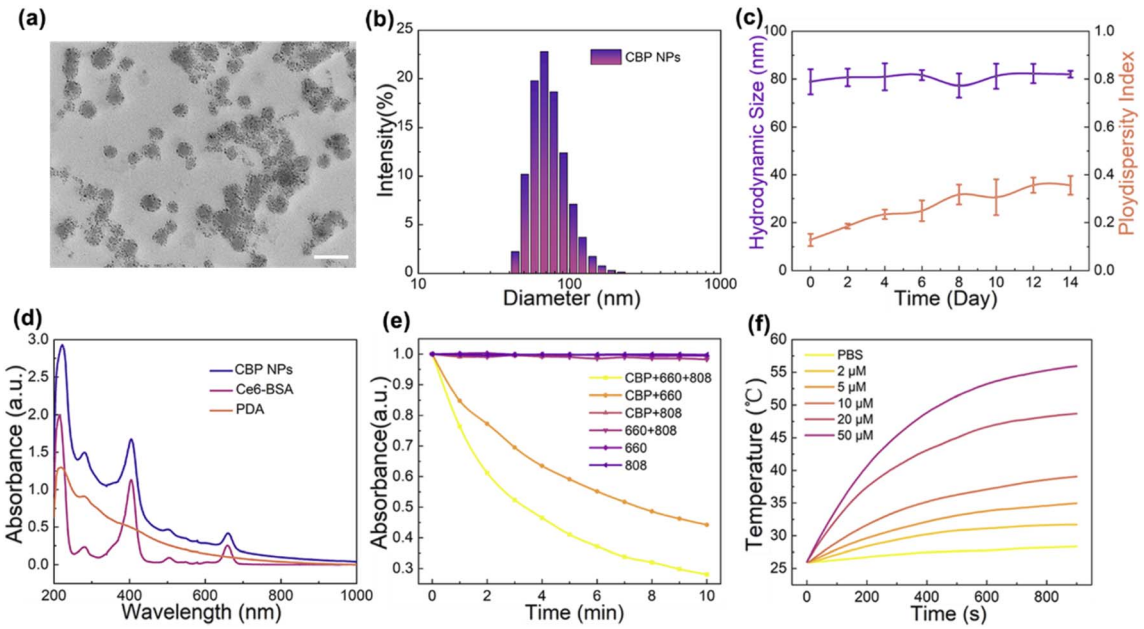

Fig. 1 Characterization of CBP NPs. (a) TEM image of CBP NPs (scale bar = 100 nm); (b) hydrodynamic diameter distribution of CBP NPs; (c) hydrodynamic diameter and PDI for 14 days in PBS buffer; (d) UV-vis-NIR absorption spectrum of CBP NPs, Ce6-BSA, and PDA; (e) normalized absorbance of ABDA during photodecomposition by ROS generation in the presence of CBP NPs or PBS under 808 nm, 660 nm or dual-mode laser exposure, respectively; (f) photothermal response of CBP NPs with different concentrations under 808 nm laser exposure.

the effect of CBP NPs under the irradiation of a 660 nm laser with/without an 808 nm laser. The power density of the 660 nm laser was 50 mW cm^{-2} and that of the 808 nm laser was 1 W cm^{-2}. As shown in Fig. 1e, the absorbance of the ABDA solution containing CBP NPs decreased after being irradiated with a single 660 nm laser and with an 808 nm laser for 10 min. However, there was no significant decline in absorbance under single 808 nm laser irradiation. Moreover, the absorbance of the pure ABDA solution as a control group did not decrease no matter which kind of laser is used for irradiation. In addition, the absorbance of ABDA was significantly reduced to 28% by double laser irradiation. In contrast, the absorbance only drops

to 44% of its initial value under the 660 nm laser alone (Fig. S2†). The results proved that CBP NPs have a good ability to produce ROS, and the effect of ROS was significantly enhanced by double laser irradiation.

PDA has strong absorption and photothermal conversion effects under 808 nm laser irradiation, which can be used for PTT. The temperature changes of different concentrations of CBP NP dispersion in PBS were measured under 808 nm laser irradiation (1 W cm^{-2}). After the laser irradiation of 800 s, the temperature of 20 μM and 50 μM CBP NP dispersions rose to 48 and 55 °C, respectively (Fig. 1f), which is sufficient to kill cancer cells. In contrast, the temperature of the deionized water in the control group changed slightly. The results proved that CBP NPs have a great photothermal effect. The stability of the photothermal response of CBP NPs was further evaluated by applying repeated cycles of laser on/off under different pH conditions. As shown in Fig. S3,† the photothermal effects of CBP NPs remained stable during four lasering cycles regardless of the difference in the pH value of the solvent.

Since PDA was reported as an acid-sensitive material for drug delivery, it is necessary to evaluate the Ce6 release from CBP NPs under the acidic and photothermal stimulus. The Ce6 release from CBP NPs was measured using the dynamic dialysis method. As shown in Fig. S4,† the Ce6 release profiles were similar under different pH conditions and the introduction of lasering could efficiently facilitate drug release possibly due to the photothermal effect of CBP NPs. In this work, Ce6 was first encapsulated into the BSA matrix *via* the nanoprecipitation method followed by protection with the PDA layer. The double layer of BSA and PDA endowed CBP NPs with enhanced structural stability and could make the NPs inert to weak acid. The enhanced drug release upon heat generation could be explained by the faster diffusion rate of Ce6 molecules rather than the damage to the NP structure. The size distribution of CBP NPs before and after light irradiation was further measured. As shown in Fig. S5,† the hydrodynamic size remained nearly identical even after a long irradiation time of 30 minutes, implying the integrity of NPs.

3.3 Cellular uptake of CBP NPs

The efficient uptake by cancer cells is a prerequisite for materials to achieve good results in cancer therapy. In order to evaluate the uptake of CBP NPs by cancer cells, we observed the intracellular fluorescence under a confocal microscope. As shown in Fig. 2a, after incubation with CBP NPs, red fluorescence signals were clearly observed in the cytoplasm of almost all cells, indicating that CBP NPs were successfully taken up by 4T1 cells. The uptake of CBP NPs by cells increased with the prolonged incubation time during 6 h. The red fluorescence signal was observed clearly after 1 h of incubation and the accumulation of CBP NPs in cells reached the peak at 4–6 h. The intracellular material content decreased gradually after 6 h, and there was almost no CBP NP residue in cells after 24 h (Fig. S6†).

Moreover, flow cytometry was used to quantitatively analyze the cellular uptake of CBP NPs. 98.9% of 4T1 cells exhibited fluorescent signals (Fig. 2b), indicating that nearly 99% of cells have taken up CBP NPs successfully. The result was highly consistent with the images taken with a confocal microscope. The above results proved that CBP NPs can be efficiently taken up by 4T1 cells.

3.4 *In vitro* biocompatibility analysis of CBP NPs

The non-toxicity or low toxicity of materials to cells is not only the basis of their application in cell experiments but also the prerequisite in cancer therapy. The CBP NPs consist of materials approved by FDA and have good biocompatibility. To evaluate the cytotoxicity of CBP NPs more accurately, the CCK-8 assay was used to evaluate the toxicity of CBP NPs to HeLa, MCF-7, MCF-10A, and 4T1 cells under different concentrations. As seen from Fig. 2c, after incubation at a high concentration of 100 μM for 24 h, more than 80% of four kinds of cells were alive.

Another important criterion to evaluate the biocompatibility of nanomaterials is the hemolysis rate. No significant hemolysis was observed within a large concentration range covering from 0 to 200 μM (Fig. S7†). The above results indicated that CBP NPs have no obvious toxicity to cells and do not cause hemolysis. CBP NPs had good biocompatibility *in vitro*, and can be used in further biological experiments.

3.5 *In vitro* photo-therapeutic effect

The PDT/PTT dual-mode therapeutic effect of CBP NPs on 4T1 cells was further investigated. After incubating with CBP NPs for 4 h, an 808 nm laser (1 W cm^{-2}) and a 660 nm laser (50 mW cm^{-2}) were used to irradiate the 4T1 cells. The intracellular ROS production was first evaluated by H2DCF-DA. As shown in Fig. S8,† cells treated with CBP NPs and light irradiation exhibited bright green fluorescence, indicating the generation of ROS inside the cells. Then, we used the CCK-8 assay to quantitatively investigate the cell survival rate. As shown in Fig. 2d, compared with the groups without CBP NP or laser treatment, the cell samples treated with CBP NPs under irradiation showed obvious death. The cell mortality was 54.2% ± 2.5% after 660 nm laser irradiation alone, 69.2% ± 1.2% after 808 nm laser irradiation alone, and 89.6% ± 2.5% after double laser irradiation.

To better visualize the PDT/PTT effect of CBP NPs on tumor cells, calcein-AM and PI were used to stain live and dead cells after treatment. As shown in Fig. 2e, all the cells in the groups without light irradiation showed high cell viability and no dead cells were observed. PDT and PTT alone contributed to partial cell death. In contrast, almost all the cells treated with CBP NPs under double laser irradiation died completely and no live cells were observed. The results were highly consistent with the CCK-8 analysis. In addition, the bright field photograph also demonstrated the cell morphology after different treatments (Fig. S9†). The above results indicated that the therapeutic effect of the combination of PDT/PTT was significantly stronger than that of PDT and PTT alone.

The synergy between PDT and PTT was further studied by calculating the combined index (CI). The therapeutic effects of PDT, PTT, and PDT&PTT based on CBP NPs were investigated by using 4T1 cells. As shown in Fig. S10,† the IC50 values of PDT,

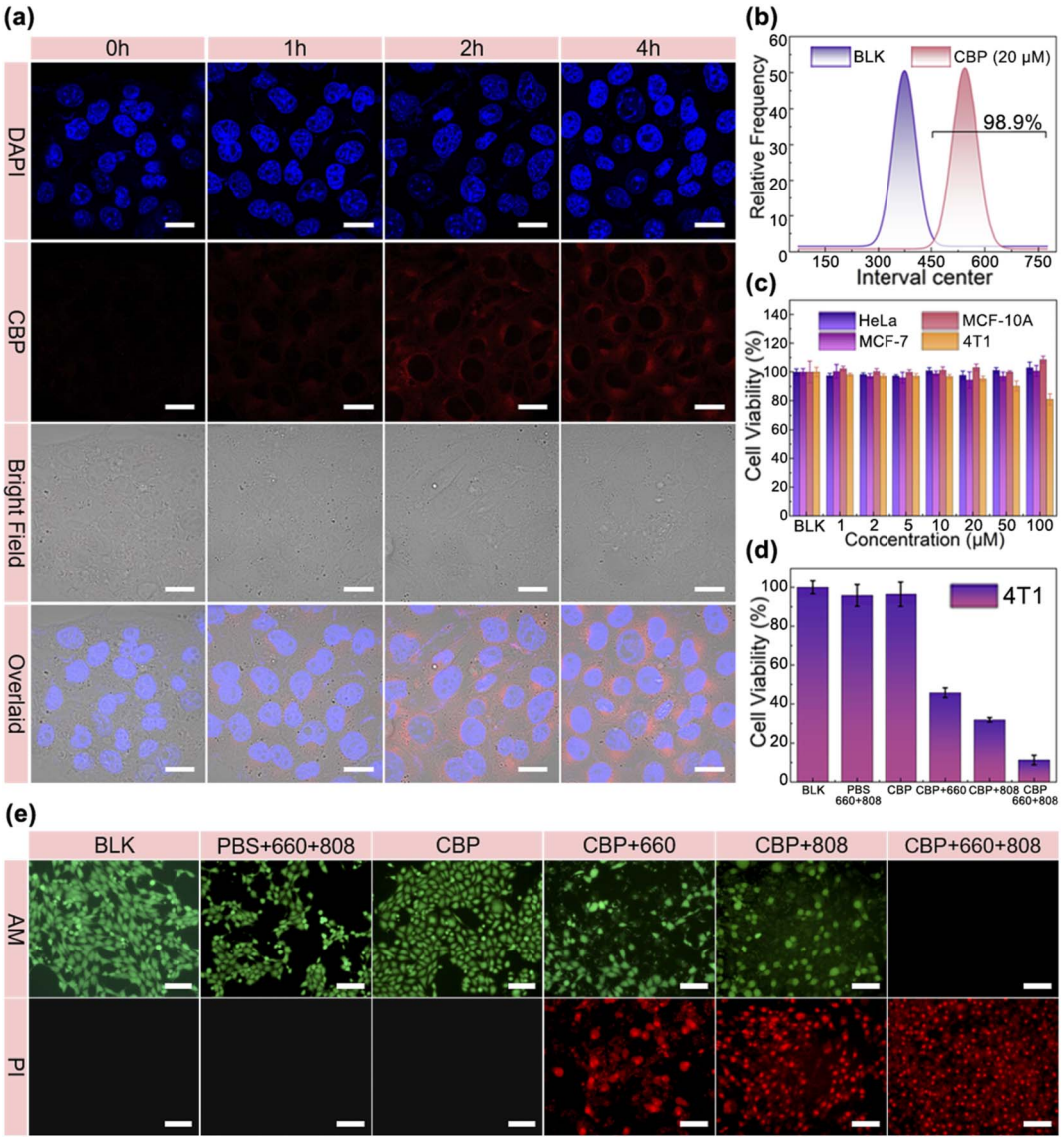

Fig. 2 Cellular uptake of CBP NPs and therapeutic effect evaluated *in vitro*. (a) Confocal fluorescence microscopy images of cells incubated with CBP NPs (scale bar = 50 μm). (b) The cellular uptake measured by flow cytometry. (c) Viability of four kinds of cells after 24 h co-incubation with CBP NPs. (d) Cell viability under different conditions of treatment. (e) Live and dead staining of cells treated under different conditions (scale bar = 200 μm).

PTT, and PDT&PTT were 15 μM, 10 μM, and 5 μM (corresponding to the concentration of Ce6), respectively. Thus, the combined index of PDT&PTT was calculated to be 5/6 (based on eqn (2)), which is smaller than 1, indicating the synergy between PDT and PTT.

3.6 *In vivo* photo-therapeutic effect

In order to further investigate the PDT/PTT dual-mode effect of CBP NPs, *in vivo* therapy experiments were performed. We established the mouse model of the subcutaneous tumor of breast cancer. 4T1 cells were inoculated subcutaneously into the right flank of Balb/C mice. When the tumor volume reached about 100 mm^3, CBP NP and laser treatments were performed.

To evaluate the temperature rise in the body, an infrared thermal imaging camera was used to record the temperature changes on the surface of the tumor under 808 nm laser (1 W cm^{-2}) irradiation. As shown in Fig. 3a and b, the temperature of the tumor area in the CBP NP treatment group increased rapidly to about 60 °C within 5 min. However, the temperature of the tumor area in the control group injected with PBS only increases slightly under the same conditions. The result indicated that CBP NPs have great photothermal conversion capability.

To investigate the therapeutic effect of CBP NPs *in vivo*, thirty tumor-bearing mice were randomly separated into 6 groups and then PBS was intratumorally injected into two groups, and CBP NPs into four groups. These four groups were further exposed to a 660 nm/808 nm/dual-mode laser at day 0. Then the body weight and tumor volume of the mice were recorded every 2

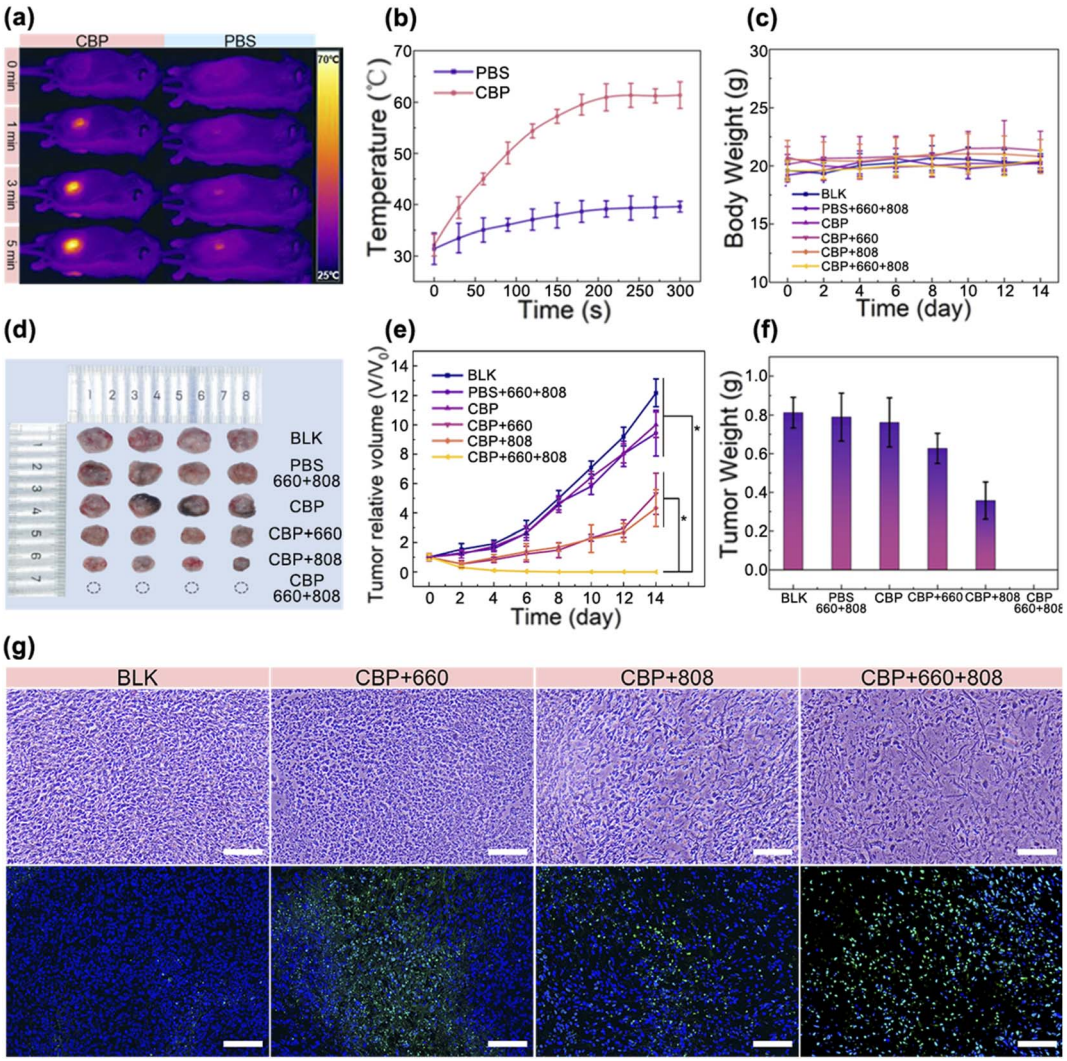

Fig. 3 *In vivo* experiment, six groups of mice were treated under different conditions. (a) *In vivo* photothermal images of tumor-bearing mice injected with PBS and CBP NP dispersion activated by an 808 nm (1 W cm^{-2}) laser for 5 min ($n = 5$). (b) Temperature increase profile of the tumor area under laser irradiation. (c) Average body weight of tumor-bearing mice in each group during the treatment periods. (d) Representative photograph of excised tumors from sacrificed mice. (e) Relative tumor volumes (compared to the whole-body volume) of tumor-bearing mice in each group. (f) Average tumor weight of treated mice in each group. (g) Representative photographs of H&E and TUNEL staining imaging of the tumor sections of tumor-bearing mice after different treatments (scale bar is 200 μm).

days. Fig. 3c and e show the changes in the mean body weight and average tumor volume over a period of 14 days. According to the results, the group treated with CBP NPs in combination with dual-mode laser irradiation had no tumor growth. In contrast, significant tumor growth was observed in the other groups. Among them, the tumor volume of the three groups of mice without phototherapy increased the fastest while mice treated with CBP NPs under single laser irradiation exhibited a slower growth rate. Furthermore, during the treatment, there was no abnormal body weight change in all groups, which preliminarily indicated that CBP NPs had good biocompatibility for *in vivo* phototherapy.

To analyze the tumor of mice after treatment, all the mice were sacrificed and their tumors were extracted. As shown in Fig. 3d, the tumor of mice treated with dual-mode phototherapy disappeared completely. By contrast, the tumor size of the three groups of mice without phototherapy was similar. The tumors of the groups treated with CBP NPs and 660 nm and 808 nm lasers alone were smaller than the former. Apart from that, we also measured the weight of the tumor in every group. The result was corresponded significantly to the tumor volume and photos discussed above (Fig. 3f).

To further investigate the cell necrosis and apoptosis in the tumor after treatment, the H&E and TUNEL staining assays were used to observe the histological changes. As shown in Fig. 3g and S11,† the images of H&E staining demonstrated that the tumor cells in the three groups without phototherapy had complete shapes and a clear outline. After PDT, PTT, and dual-mode phototherapy, the morphology of tumor cells changed significantly, including decreased cell density, karyopyknosis, karyorrhexis, and karyolysis. The images of TUNEL demonstrate that all the tumor cells undergo apoptosis after the treatment

with CBP NPs in combination with double laser irradiation, while there was nearly no apoptosis in the groups without phototherapy.

The above results indicated that compared with the therapeutic effects of PDT and PTT alone, the dual-mode therapy of PTT/PDT based on CBP NPs has a better therapeutic effect on cancer and can significantly reduce the volume and weight of the tumor.

3.7 *In vivo* biocompatibility analysis of CBP

In order to further investigate the biocompatibility of CBP NPs *in vivo*, a complete and systematic assay was performed. Twenty mice were randomly separated into four groups. PBS buffer and CBP NP dispersions with low (1 mg kg^{-1}), medium (10 mg kg^{-1}) and high (30 mg kg^{-1}) concentrations were injected into the tail vein, respectively. The body weight of the mice was recorded every 2 days. The results show that the body weight of all the mice in the four groups remained stable during 14 days. Meanwhile, there was no statistical difference in the body weight between the experimental group and the control group (Fig. S12†). To analyze the blood routine and blood biochemical analysis and observe the organ structure, all the mice were sacrificed, and their blood and organs were extracted after observation for 14 days. As shown in Fig. 4a and b, there was no statistical difference in blood routine and blood biochemical indexes between the four groups. The results showed that the CBP NPs cannot cause abnormal metabolism and blood dysfunction, and cannot affect the function of main organs, blood lipids, and normal physiological and biochemical reactions *in vivo*. In addition, we sectioned the main organs (heart, liver, spleen, lung, and kidney) of each group of mice and calculated the organ coefficients. As shown in Fig. 4c and S13,† obvious transverse striation and branches can be seen in the heart section, the central segment is cylindrical, and the nucleus was located in the center of the cell; large, round, and centered nuclei can be seen in the liver section, and the chromatin was rich; clear white pulp, red pulp, and the marginal zone can be seen in the spleen section; clear reticular structure

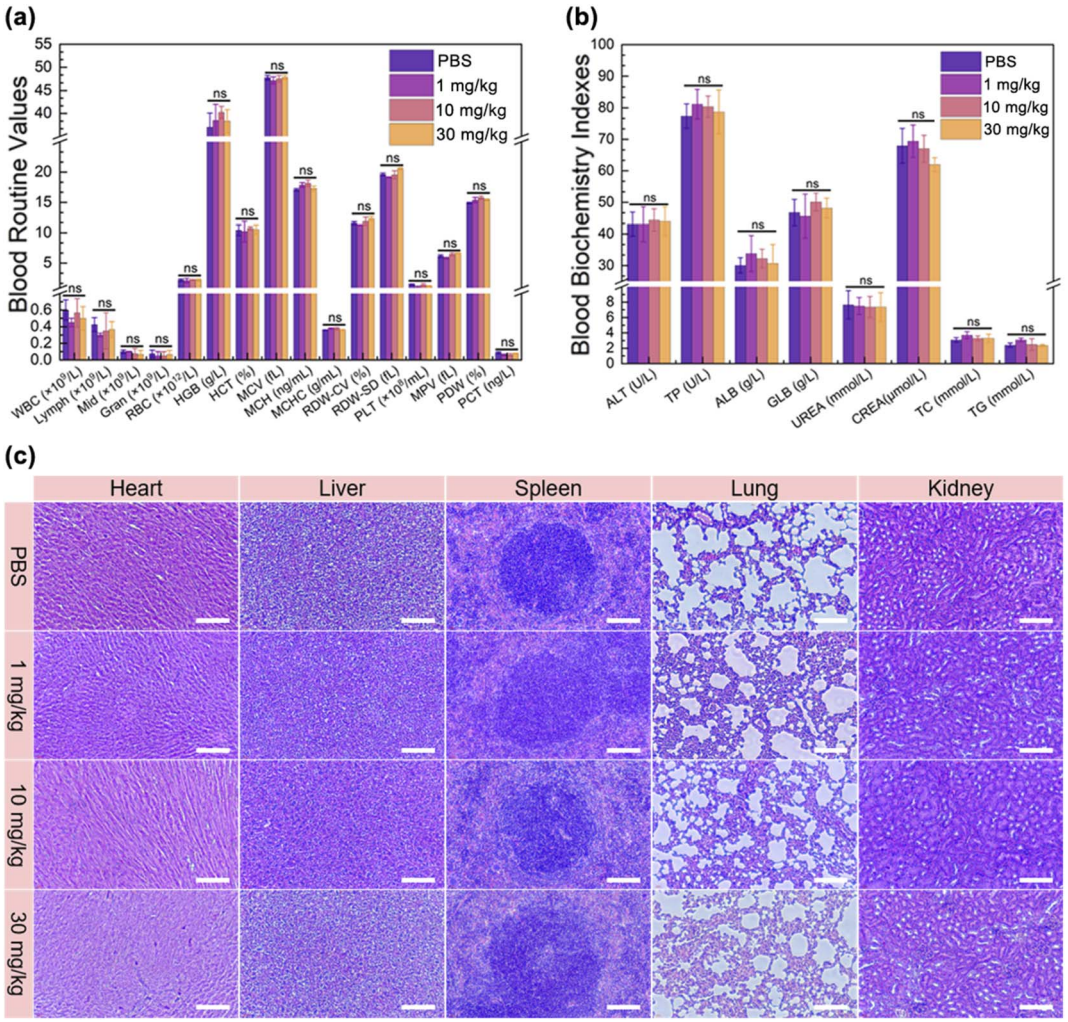

Fig. 4 Biocompatibility analysis of CBP NPs *in vivo* ($n = 5$). (a) Blood routine values of our groups of mice injected with PBS solution, CBP NP suspensions with low, medium and high concentrations, respectively; (b) blood biochemistry indexes of four groups of mice; (c) representative photograph of main organ sections of four groups of mice.

can be seen in the lung section, and the nucleus and cytoplasm were in sharp contrast; normal glomerular size and shape, clear boundary, and no inflammatory cell infiltration in the renal interstitium can be seen in the kidney section; the brush-like margin inside the renal tubules was intact; there was no statistical difference in organ coefficients among the four groups. The results indicated that there were no pathological changes nor damage in the main organs of the four groups, and the cell morphology was normal and intact.

In general, our experimental results strongly proved that the dual-mode therapy of PTT/PDT based on CBP NPs not only had an excellent tumor therapeutic effect but also had high biocompatibility *in vivo*.

4 Conclusions

In this contribution, CBP NPs, a biocompatible photo-therapeutic agent, which are composed of FDA-approved ingredients Ce6 and PDA, were successfully designed and synthesized for enhanced cancer phototherapy *via* a facile modified nano-precipitation method. According to a series of systematic and comprehensive experiments, CBP NPs have been proven to have an efficient therapeutic effect on 4T1 cancer cells and high biocompatibility *in vivo* and *in vitro*. Specifically, under the dual-mode irradiation of an 808 nm laser (1 W cm^{-2}) and a 660 nm laser (50 mW cm^{-2}) at low power density, CBP NPs with a low concentration (20 μM) have still demonstrated an efficient anti-cancer effect. Such a highly boosted photo-therapeutic effect originated from the synergistic effect of ROS and hyperthermia. More importantly, CBP NPs have demonstrated great biocompatibility and negligible toxicity in tumor-bearing animal therapeutic trials. In brief, our nanoprobe has the advantages of on-demand control, minimum invasiveness, and lower side effects, and is a good candidate for the combined PDT/PTT therapy in future translational medicine.

Conflicts of interest

The authors declare that they have no known competing financial interests or personal relationships that could have appeared to influence the work reported in this paper.

Acknowledgements

This work was supported by the National Natural Science Foundation of China (31871442) and the Natural Science Foundation of Guangdong Province (2021A1515012159). The authors greatly appreciate the Instrumental Analysis Center of Shenzhen University for assistance with imaging analysis. Animal experiments were carried out in accordance with the regulations of the Animal Ethical and Welfare Committee of Shenzhen University (AEWC-SZU).

References

1 R. L. Siegel, *et al.*, Cancer Statistics, 2021, *Ca-Cancer J. Clin.*, 2021, **71**, 7–33.
2 F. Islami, *et al.*, Annual Report to the Nation on the Status of Cancer, Part 1: National Cancer Statistics, *J. Natl. Cancer Inst.*, 2021, **113**(12), 1648–1669.
3 S. J. Henley, *et al.*, Annual report to the nation on the status of cancer, part I: National Cancer Statistics, *Cancer*, 2020, **126**(10), 2225–2249.
4 W. Yun, *et al.*, A depression and anxiety in relation to cancer incidence and mortality: a systematic review and meta-analysis of cohort studies, *Mol. Psychiatry*, 2020, **25**, 1487–1499.
5 H. Sung and J. Ferlay, Global cancer statistics 2020: GLOBOCAN estimates of incidence and mortality worldwide for 36 cancers in 185 countries, *CA: Cancer J. Clin.*, 2021, **71**(3), 209–249.
6 G. Song and L. Cheng, Emerging nanotechnology and advanced materials for cancer radiation therapy, *Adv. Mater.*, 2017, **29**(32), 1700996.
7 Y. Liu and P. Bhattarai, Photothermal therapy and photoacoustic imaging via nanotheranostics in fighting cancer, *Chem. Soc. Rev.*, 2019, **48**(7), 2053–2108.
8 D. Kashyap, Natural product-based nanoformulations for cancer therapy: opportunities and challenges, *Semin. Cancer Biol.*, 2021, **69**, 5–23.
9 W. Fan and P. Huang, Overcoming the Achilles' heel of photodynamic therapy, *Chem. Soc. Rev.*, 2016, **45**(23), 6488–6519.
10 G. Wei and Y. Wang, Recent progress in nanomedicine for enhanced cancer chemotherapy, *Theranostics*, 2021, **11**(13), 6370–6392.
11 Z. Xie, *et al.*, Emerging combination strategies with phototherapy in cancer nanomedicine, *Chem. Soc. Rev.*, 2020, **49**(22), 8065–8087.
12 J. P. E. A. Celli, Imaging and photodynamic therapy:mechanisms, monitoring, and optimization, *Chem. Rev.*, 2010, **110**, 2795–2838.
13 D. E. F. D. Dolmans, Photodynamic therapy for cancer, *Nat. Rev. Cancer*, 2003, **3**, 380–387.
14 A. Juarranz and J. P. S., Photodynamic therapy of cancer. Basic principles and applications, *Clin. Transl. Oncol.*, 2008, **10**, 148–154.
15 K. H. M. B. Richter, The heat shock response: life on the verge of death, *Mol. Cell*, 2010, **40**, 253–266.
16 E. M. Knavel and C. L. Brace, Tumor ablation: common modalities and general practices, *Tech. Vasc. Interv. Radiol.*, 2013, **16**, 192–200.
17 C. M. Goodman, C. D. McCusker, T. Yilmaz, *et al.*, Toxicity of gold NPs functionalized with cationic and anionic side chains, *Bioconjugate Chem.*, 2004, **15**, 897–900.
18 A. Magrez, S. Kasas, V. Salicio, *et al.*, Cellular toxicity of carbon-based nanomaterials, *Nano Lett.*, 2006, **6**, 1121–1125.
19 Z. M. E. A. Tang, Pyroelectric nanoplatform for NIR-II-triggered photothermal therapy with simultaneous pyroelectric dynamic therapy, *Mater. Horiz.*, 2018, **5**, 946–952.
20 Q. F. E. A. Xiao, A core/satellite multifunctional nanotheranostic for in vivo imaging and tumor eradication

by radiation/photothermal synergistic therapy, *J. Am. Chem. Soc.*, 2013, **135**, 13041–13048.

21 B. W. C. Z. Tian, Photothermally enhanced photodynamic therapy delivered by nano-graphene oxide, *ACS Nano*, 2011, **5**, 7000–7009.

22 A. H. K. A. Hawasli, Stereotactic laser ablation of high-grade gliomas, *Neurosurg. Focus*, 2014, **37**, FOCUS14471.

23 S. C. S. E. Lal, Nanoshell-enabled photothermal cancer therapy: impending clinical impact, *Acc. Chem. Res.*, 2008, **41**, 1842–1851.

24 A. R. E. A. Rastinehad, Gold nanoshell-localized photothermal ablation of prostate tumors in a clinical pilot device study, *Proc. Natl. Acad. Sci*, 2019, **116**, 18590–18596.

25 Z. Xu, *et al.*, NIR-II-activated biocompatible hollow nanocarbons for cancer photothermal therapy, *J. Nanobiotechnol.*, 2021, **19**(1), 1842–1851.

26 N. Panwar, G. X. Xu, *et al.*, Nanocarbons for Biology and Medicine: Sensing, Imaging, and Drug Delivery, *Chem. Rev.*, 2019, **119**(16), 9559–9656.

27 B. Gu and G. X. Xu, Precise Two-Photon Photodynamic Therapy using an Efficient Photosensitizer with Aggregation-Induced Emission Characteristics, *Adv. Mater.*, 2017, **29**(28), 201701076.

28 Z. Cheng, *et al.*, Nanomaterials for cancer therapy: current progress and perspectives, *J. Hematol. Oncol.*, 2021, **14**(1), 85.

29 D. Cui, F. Tian, C. S. Ozkan, M. Wang and H. Gao, Effect of single wall carbon nanotubes on human HEK293 cells, *Toxicol. Lett.*, 2005, **155**(1), 73–85.

30 C. M. Sayes, A. M. Gobin, K. D. Ausman, J. Mendez, J. L. West and V. L. Colvin, Nano-C60 cytotoxicity is due to lipid peroxidation, *Biomaterials*, 2005, **26**(36), 7587–7595.

31 K. Pulskamp, S. Diabate and H. F. Krug, Carbon nanotubes show no sign of acute toxicity but induce intracellular reactive oxygen species in dependence on contaminants, *Toxicol. Lett.*, 2007, **168**(1), 58–74.

32 X. Yuan, *et al.*, Cellular Toxicity and Immunological Effects of Carbon-based Nanomaterials, *Part. Fibre Toxicol.*, 2019, **16**, 18.

33 A. Ormond and H. Freeman, Dye Sensitizers for Photodynamic Therapy, *Mater.*, 2013, **6**(3), 817–840.

34 F. Ding, *et al.*, Polydopamine-coated Nucleic Acid Nanogel for siRNA-Mediated Low-Temperature Photothermal Therapy, *Biomaterials*, 2020, **245**, 119976.